Vietnam Journal of Mechanics, Vol. 45, No. 3 (2023), pp. 259 – 272
DOI: https://doi.org/10.15625/0866-7136/19027

A POLYGONAL FINITE ELEMENT METHOD FOR SHAKEDOWN ANALYSIS OF STRUCTURES

Phuc L. H. Ho[1], Canh V. Le[2,3*], Phuong H. Nguyen[1], Dung T. Tran[4]
[1]*University Core Research Center for Disaster-free & Safe Ocean City Construction, Dong-A University, Busan, 49315, South Korea*
[2]*School of Civil Engineering and Management, International University, Ho Chi Minh City, Vietnam*
[3]*Vietnam National University, Ho Chi Minh City, Vietnam*
[4]*Faculty of Civil Engineering, Ho Chi Minh City Open University, Ho Chi Minh City, Viet Nam*
[*]E-mail: lvcanh@hcmiu.edu.vn

Received: 13 March 2023 / Published online: 30 September 2023

Abstract. This study presents an innovative numerical method that combines the polygonal finite element method (Poly-FEM) with conic optimization techniques within the framework of structural shakedown analysis. The resulting optimization problem is formulated as a second-order cone programming (SOCP) problem and is efficiently solved using the MOSEK primal-dual interior-point solver. Numerical experiments validate the computational efficiency and efficacy of the proposed approach.

Keywords: polygonal finite element method, shakedown analysis, cyclic load, second-order cone programming.

1. INTRODUCTION

Shakedown analysis, employed in civil, aerospace, and mechanical engineering, evaluates structural responses to cyclic loads. It optimizes designs, predicts fatigue life, and ensures long-term structural integrity, enhancing safety and efficiency across engineering applications.

Building upon Koiter's [1] and Melan's [2] bounding theorems, numerical shakedown analysis involves solving an intricate min/max optimization problem characterized by nonlinear constraints. Initial methods, including piecewise-linear yield criteria

and Newton-type schemes [3–5], were computationally demanding due to intricate calculations. The interior-point method later emerged as an efficient algorithm for large-scale engineering problems [6, 7], primarily applied to the von Mises yield criterion. Recent advancements in plastic analysis have significantly expanded shakedown analysis capabilities. Andersen [8] notably introduced a primal-dual interior-point algorithm with second-order cones, enhancing shakedown analysis potential. Subsequent studies, conducted by researchers including [9–13], have provided further validation of these advancements.

Simultaneously, numerical techniques have evolved to enhance the computational efficiency of shakedown analysis. Significantly, the standard finite element method (FEM) [4, 10, 14–17] has played a pivotal role in this domain. Another approach, known as isogeometric analysis (IGA), has also emerged [18]. Complementing FEM advancements, smoothed finite element methods (S-FEMs) have found application in this context [11, 19, 20]. Additionally, mesh-free methods have been effectively employed in shakedown analysis, as seen in the nodal natural element method [21] and the stabilized integrated radial basis function method [12].

When tackling complex problems, studies have shown that polygonal elements outperform traditional triangular and quadrilateral elements in mesh design [22–24]. Building upon the foundation of Wachspress shape functions, originally introduced by [25], numerous numerical approaches have been developed over the years to create polygonal/polyhedral finite elements. These approaches include the Voronoi cell finite element method (VCFEM), Hybrid polygonal element (HPE), n-Sided polygonal smoothed finite element method (nSFEM), Polygonal scaled boundary finite element method (PSBFEM), Virtual node method (VNM), among others. Polygon-based finite element methods have found extensive applications in various fields of mechanics, including elasticity analysis [24, 26], simulations of crack growth [27], topology optimization [28, 29], and many other areas.

This study aims to develop an efficient and resilient numerical approach for kinematic shakedown analysis of structures. This is accomplished by integrating the polygonal finite element method with conic programming, where the optimization problem is formulated in a conic manner to effectively reduce its size. High-performance interior-point solvers are employed to swiftly determine shakedown limits. Rigorous comparisons with reference results from the literature are carried out to assess the accuracy and convergence rate of the obtained solutions. These assessments are based on numerical investigations conducted on a benchmark structure subjected to monotonic and repeated loads. Furthermore, the distribution of dissipation work is employed to predict collapse mechanisms, offering practical insights for structural design at the limit state and enhancing the practical relevance of this study.

2. KINEMATIC SHAKEDOWN FORMULATION

Consider an elastic-perfectly plastic body with an area denoted as Ω. This body has a kinematic boundary Γ_u, a static boundary Γ_t, and is subjected to cyclic loads $\mathbf{t}$. Based on Koiter's kinematic theorem, the shakedown analysis formulation can be mathematically expressed as follows

$$\begin{aligned} \lambda_{sd}^{+} &= \min_{\boldsymbol{\epsilon}^p,\mathbf{u}} \int_t \int_\Omega \mathcal{D}(\boldsymbol{\epsilon}^p)\, \mathrm{d}\Omega \mathrm{d}t, \\ \text{s.t} &\begin{cases} \int_t \int_\Omega (\boldsymbol{\sigma}^e)^{\mathrm{T}} \boldsymbol{\epsilon}^p \, \mathrm{d}\Omega \mathrm{d}t = 1, \\ \Delta\boldsymbol{\epsilon} = \int_t \boldsymbol{\epsilon}^p \, \mathrm{d}t, & \text{in } \Omega \\ \mathbf{u} = 0, & \text{on } \Gamma_u \end{cases} \end{aligned} \tag{1}$$

where $\lambda_{\mathrm{sd}}^{+}$ signifies the upper bound shakedown load multiplier, $\mathcal{D}(\boldsymbol{\epsilon}^p)$ represents the plastic dissipation rate associated with the plastic strain rate $\boldsymbol{\epsilon}^p$, $\Delta\boldsymbol{\epsilon}$ is the accumulative admissible plastic strain rate at the end of a loading cycle $t \in [0, T]$, $\boldsymbol{\sigma}^e$ is the related fictitious elastic stress, and $\mathbf{u}$ is the displacement velocity.

This study employs the von Mises yield criterion, which can be mathematically expressed in terms of second-order polynomials as

$$\varphi(\boldsymbol{\sigma}) = \sqrt{\boldsymbol{\sigma}^{\mathrm{T}} \mathbf{P} \boldsymbol{\sigma}} - \sigma_p, \tag{2}$$

where, φ is the yield function linked to the yield stress σ_p, while the matrix $\mathbf{P}$ represents the coefficients associated with the material's strength properties.

Let $\boldsymbol{\Theta}$ denote the inverse of $\mathbf{P}$, which is given by the following matrix for a plane stress problem

$$\boldsymbol{\Theta} = \frac{1}{3} \begin{bmatrix} 4 & 2 & 0 \\ 2 & 4 & 0 \\ 0 & 0 & 1 \end{bmatrix}. \tag{3}$$

The plastic dissipation power can be computed using the following expression

$$\mathcal{D}(\boldsymbol{\epsilon}^p) = \sigma_p \sqrt{(\boldsymbol{\epsilon}^p)^{\mathrm{T}} \boldsymbol{\Theta} \boldsymbol{\epsilon}^p}. \tag{4}$$

To simplify the time-dependent integration in the shakedown formulation (1), Konig's two convex theorems [30] can be applied. These theorems state that it is sufficient to evaluate the shakedown limits at the vertices of the convex polyhedral load domain. Consequently, the optimization problem (1) can be reformulated as

$$\lambda_{sd}^{+} = \min_{\boldsymbol{\epsilon}^p, \mathbf{u}} \sum_{j=1}^{\mathcal{N}_v} \int_{\Omega} \sigma_p \sqrt{(\boldsymbol{\epsilon}^p)^{\mathrm{T}} \boldsymbol{\Theta} \boldsymbol{\epsilon}^p} \mathrm{d}\Omega,$$

$$\text{s.t} \begin{cases} \mathbf{u} = 0, & \text{on } \Gamma_u \\ \Delta\boldsymbol{\epsilon} = \sum_{j=1}^{\mathcal{N}_v} \boldsymbol{\epsilon}_j^p, & \text{in } \Omega \\ \sum_{j=1}^{\mathcal{N}_v} \int_{\Omega} \left(\boldsymbol{\sigma}_j^e\right)^{\mathrm{T}} \boldsymbol{\epsilon}_j^p \, \mathrm{d}\Omega = 1. \end{cases} \tag{5}$$

In this reformulation (5), $\mathcal{N}_v$ represents the number of vertices of the convex polyhedral load domain $\mathcal{L}$. Notably, the shakedown formulation (5) reduces to the limit analysis problem when considering only one load vertex.

3. A BRIEF REVIEW ON POLYGONAL FINITE ELEMENT METHOD

Consider a polygonal master element denoted as Ω^e, which possesses $\mathcal{N}$ vertices, denoted as $\{\mathbf{x}_1, \mathbf{x}_2, \ldots, \mathbf{x}_{\mathcal{N}}\}$. These vertices are arranged in a counter-clockwise manner, where $\mathbf{x}_i = \left(\cos\frac{2\pi i}{\mathcal{N}}, \sin\frac{2\pi i}{\mathcal{N}}\right)$, for $i = 1, 2, \ldots, \mathcal{N}$ and $\mathcal{N} \geq 3$. Among the various polygonal shape functions proposed in the existing literature, this study focuses on the utilization of Wachspress coordinates, which provide a straightforward and efficient means for constructing shape functions on convex polygons [31]. It should be noted that Wachspress coordinates represent the lowest-order barycentric coordinates that simultaneously satisfy the properties of boundedness, linearity along the edges, and linear independence within convex polygons [32].

For any given point $\boldsymbol{\xi}(r, s)$ within Ω^e, the Wachspress shape functions is defined as follows

$$\psi_i(\boldsymbol{\xi}) = \frac{\omega_i(\boldsymbol{\xi})}{\sum_{j=1}^{\mathcal{N}} \omega_j(\boldsymbol{\xi})}, \quad \text{with} \quad \omega_i(\boldsymbol{\xi}) = \frac{A\left(\mathbf{x}_{i-1}, \mathbf{x}_i, \mathbf{x}_{i+1}\right)}{A\left(\boldsymbol{\xi}, \mathbf{x}_{i-1}, \mathbf{x}_i\right) A\left(\boldsymbol{\xi}, \mathbf{x}_i, \mathbf{x}_{i+1}\right)}, \tag{6}$$

where $A\left(\mathbf{x}_\alpha, \mathbf{x}_\beta, \mathbf{x}_\gamma\right)$ represents the signed area of the triangle formed by nodes $\left(\mathbf{x}_\alpha, \mathbf{x}_\beta, \mathbf{x}_\gamma\right)$, as depicted in Fig. 1.

As the polygonal master element is regular in shape, the area $A\left(\mathbf{x}_{i-1}, \mathbf{x}_i, \mathbf{x}_{i+1}\right)$ consistent for all vertices and can be factored out of the expression in Eq. (6). The weight function $\omega_i(\boldsymbol{\xi})$ can be reformulated as follows

$$\omega_i(\boldsymbol{\xi}) = \frac{1}{A_i(\boldsymbol{\xi})\, A_{i+1}(\boldsymbol{\xi})}, \tag{7}$$

where the triangular area $A_i(\boldsymbol{\xi})$ can be determined by:

$$A_i(\boldsymbol{\xi}) = A\left(\boldsymbol{\xi}, \mathbf{x}_{i-1}, \mathbf{x}_i\right) = \frac{1}{2}\begin{vmatrix} r & s & 1 \\ x_{i-1}^{(1)} & x_{i-1}^{(2)} & 1 \\ x_i^{(1)} & x_i^{(2)} & 1 \end{vmatrix}. \tag{8}$$

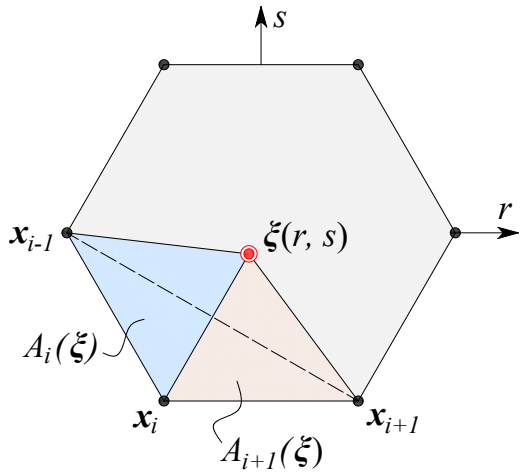

Fig. 1. Illustration of triangle areas used to define the Wachspress coordinates in the master element

The derivatives of the shape functions can be calculated as follows

$$\frac{\partial \psi_i(\boldsymbol{\xi})}{\partial r} = \frac{1}{\sum_{j=1}^{\mathcal{N}} \omega_j(\boldsymbol{\xi})}\left[\frac{\partial \omega_i(\boldsymbol{\xi})}{\partial r} - \psi_i(\boldsymbol{\xi}) \sum_{j=1}^{\mathcal{N}} \frac{\partial \omega_j}{\partial r}\right], \tag{9a}$$

$$\frac{\partial \psi_i(\boldsymbol{\xi})}{\partial s} = \frac{1}{\sum_{j=1}^{\mathcal{N}} \omega_j(\boldsymbol{\xi})}\left[\frac{\partial \omega_i(\boldsymbol{\xi})}{\partial s} - \psi_i(\boldsymbol{\xi}) \sum_{j=1}^{\mathcal{N}} \frac{\partial \omega_j}{\partial s}\right], \tag{9b}$$

where

$$\frac{\partial \omega_j}{\partial r} = -\omega_j(\boldsymbol{\xi})\left[\frac{1}{A_j(\boldsymbol{\xi})}\frac{\partial A_j(\boldsymbol{\xi})}{\partial r} + \frac{1}{A_{j+1}(\boldsymbol{\xi})}\frac{\partial A_{j+1}(\boldsymbol{\xi})}{\partial r}\right], \tag{10a}$$

$$\frac{\partial \omega_j}{\partial s} = -\omega_j(\boldsymbol{\xi})\left[\frac{1}{A_j(\boldsymbol{\xi})}\frac{\partial A_j(\boldsymbol{\xi})}{\partial s} + \frac{1}{A_{j+1}(\boldsymbol{\xi})}\frac{\partial A_{j+1}(\boldsymbol{\xi})}{\partial s}\right], \tag{10b}$$

where

$$\frac{\partial A_j(\boldsymbol{\xi})}{\partial r} = \frac{1}{2}\left(x_{j-1}^{(2)} - x_j^{(2)}\right), \quad \frac{\partial A_j(\boldsymbol{\xi})}{\partial s} = \frac{1}{2}\left(x_{j-1}^{(1)} - x_j^{(1)}\right). \tag{11}$$

In Fig. 2, the Wachspress shape function for the hexagonal master element is depicted. It's crucial to emphasize that the Wachspress shape functions, as defined in Eq. (6), exhibit several fundamental characteristics essential for finite element analysis. These characteristics encompass non-negativity, adherence to the partition of unity, compliance

with the Kronecker delta condition, linear completeness within the element's domain, and linear interpolation between neighboring nodes along all element boundaries [33].

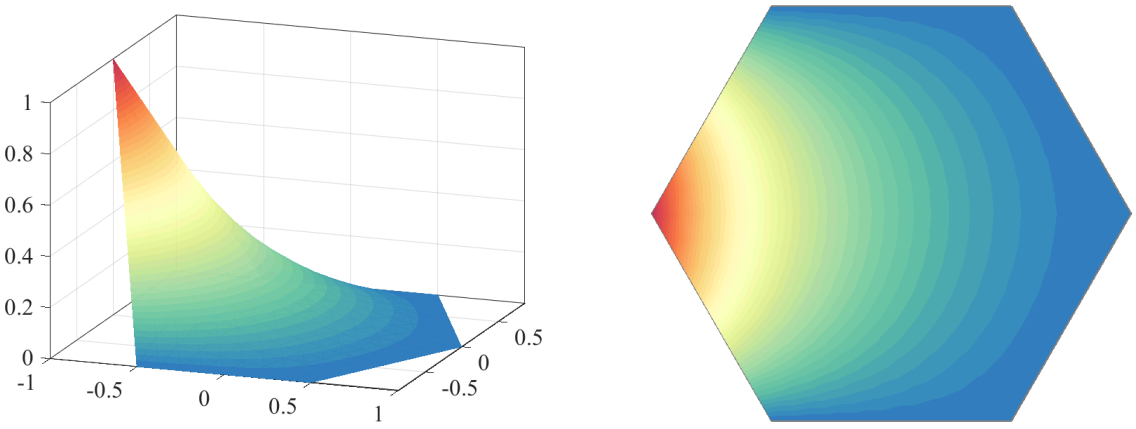

(a) The Wachspress shape function (b) The contour of Wachspress shape function

Fig. 2. The Wachspress shape function for the hexagonal master element

4. NUMERICAL DISCRETIZATION USING POLY-FEM AND SOCP

Using the Poly-FEM approach, the displacement field is approximated as

$$\mathbf{u}^h(\mathbf{x}) = \mathbf{N}(\mathbf{x})\mathbf{d}, \tag{12}$$

where, $\mathbf{N}$ represents the Wachspress shape functions as defined in Eq. (6), and $\mathbf{d}$ is the displacement vector given by

$$\mathbf{d}^{\mathrm{T}} = [u_1, v_1, \ldots, u_{\mathcal{N}_{nod}}, v_{\mathcal{N}_{nod}}], \tag{13}$$

where $\mathcal{N}_{nod}$ is the number of discretized nodes in the computational domain.

The strain rate is then calculated as

$$\boldsymbol{\epsilon}^p = \mathbf{B}\mathbf{d}, \tag{14}$$

where $\mathbf{B}$ represents the strain-displacement matrix consisting of the derivatives of shape function.

The fictitious elastic stress $\boldsymbol{\sigma}^e$ can be determined using Hooke's law, which relates stress to strain through the following equation:

$$\boldsymbol{\sigma}^e = \mathbf{D}\boldsymbol{\epsilon} = \mathbf{D}\mathbf{B}\mathbf{d}, \tag{15}$$

where $\mathbf{D}$ denotes the constitutive matrix.

Plastic dissipation can be expressed as a sum of norms

$$\mathcal{D}(\boldsymbol{\epsilon}^p) = \sigma_p \sum_{j=1}^{\mathcal{N}_v} \sum_{k=1}^{\mathcal{N}_g} \zeta_k \|\boldsymbol{\rho}_{jk}\|, \tag{16}$$

where $\mathcal{N}_g$ is the number of integration points, ζ_k represents the integration weight at the point k, and $\|\cdot\|$ denotes the Euclidean norm, i.e., $\|\mathbf{x}\| = \sqrt{\mathbf{x}^{\mathrm{T}}\mathbf{x}}$. The additional variables $\boldsymbol{\rho}_{jk}$ for the plane stress problem can be defined as

$$\boldsymbol{\rho}_{jk} = \begin{bmatrix} \rho_1 \\ \rho_2 \\ \rho_3 \end{bmatrix} = \frac{1}{\sqrt{3}} \begin{bmatrix} 2 & 0 & 0 \\ 1 & \sqrt{3} & 0 \\ 0 & 0 & 1 \end{bmatrix}. \tag{17}$$

Let $\mathbf{t}_{jk}$ be the auxiliary variable belonging to the standard conic constraint defined as

$$\mathcal{C} = \left\{ \mathbf{x} \in \mathbb{R}^n \mid x_1 \geq \sqrt{x_2^2 + x_3^2 + \cdots + x_n^2} \right\}. \tag{18}$$

The kinematic shakedown analysis problem (5) can be formulated as a second-order cone programming problem as follows

$$\begin{aligned} \lambda^{sd} \quad = \quad & \min_{\boldsymbol{\epsilon}_j^p, \mathbf{u}} \sum_{j=1}^{\mathcal{N}_v} \sum_{k=1}^{\mathcal{N}_s} \sigma_p \zeta_k t_{jk}, \\ \text{s.t} \quad & \begin{cases} \mathbf{d} = \mathbf{0}, \quad \text{on } \Gamma_u \\ \Delta\boldsymbol{\epsilon}_j^p = \sum_{j=1}^{\mathcal{N}_v} \mathbf{B}\mathbf{d}, \\ \sum_{j=1}^{\mathcal{N}_v} \sum_{k=1}^{\mathcal{N}_s} \left(\boldsymbol{\sigma}_{jk}^e\right)^{\mathrm{T}} \boldsymbol{\epsilon}_{jk}^p = 1, \\ \|\boldsymbol{\rho}_{jk}\| \leq t_{jk}, \; j = 1 \ldots \mathcal{N}_v, \; k = 1 \ldots \mathcal{N}_g. \end{cases} \end{aligned} \tag{19}$$

5. NUMERICAL RESULTS

In this section, a numerical investigation is conducted to evaluate the performance of the proposed method under plane stress conditions and various specified load combinations. To solve the formulated optimization problems, the academic MOSEK software package [34] is employed, and integrated into the MATLAB environment. The computations take place on a 3.2 GHz Intel Core i9 PC running Windows 11.

Consider a square plate with a central circular cutout subjected to in-plane traction forces (p_1, p_2), as depicted in Fig. 3(a). Noteworthy input parameters for this analysis include $R = 1$ m, $A = 5R$, $E = 2.1 \times 10^5$ MPa, $\nu = 0.3$, and $\sigma_p = 250$ MPa. To simplify the analysis, only the upper-right quarter of the plate is modeled due to geometric symmetry,

as shown in Fig. 3(b). Fig. 3(c) visually represents the computational domain discretized using 193 polygonal elements.

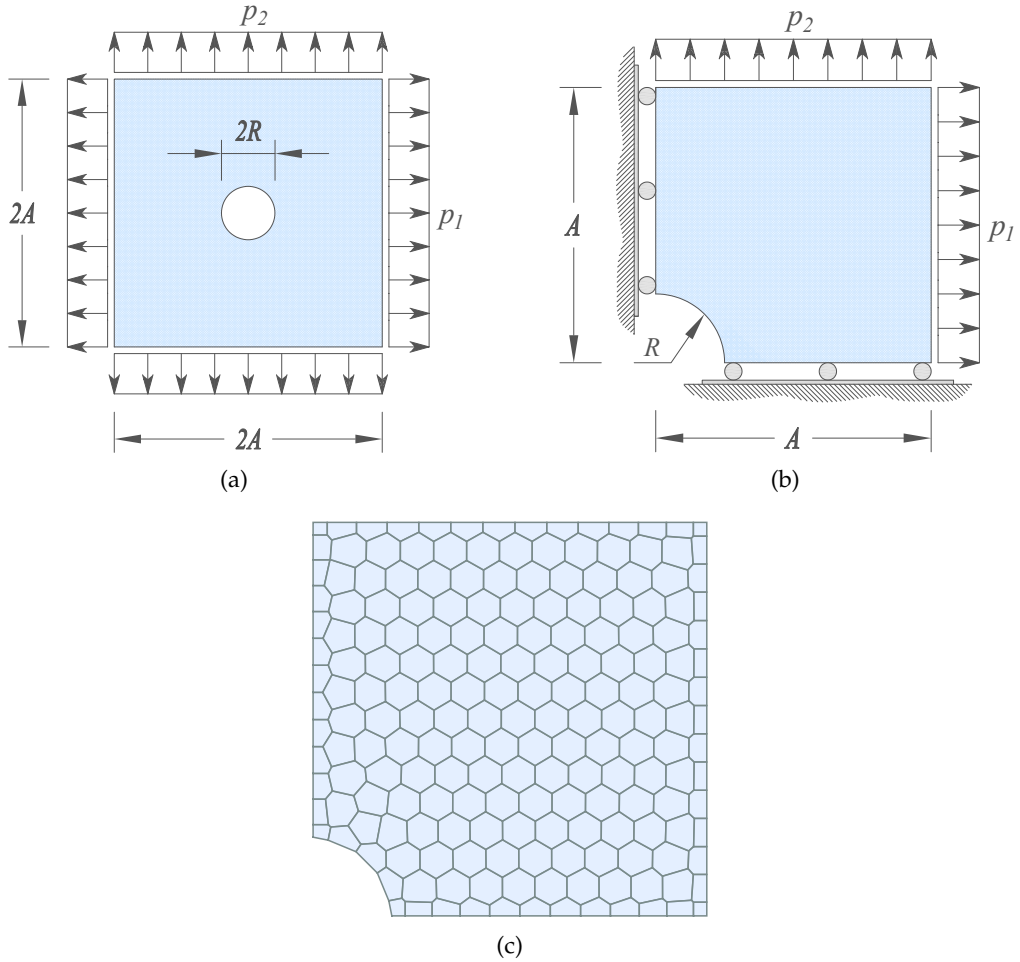

Fig. 3. Plate hole problem: (a) Geometry, dimensions, and loading; (b) Computational domain; (c) Finite element discretization

5.1. Plate under monotonous loads

Initially, the investigation focuses on the plate's response to a proportionally increasing single load p_1 to assess the accuracy and convergence of the proposed method. An analytical solution for this loading scenario is available, as reported in [35], expressed as $\lambda_{\text{lm}}^{\text{e}} = 0.800 \times \frac{p_1}{\sigma_p}$. Table 1 summarizes the computed limit load multipliers λ_{lm}^{+} for various mesh resolutions. The convergence of these numerical results is further illustrated

in Fig. 4. It's worth noting that as the number of variables increases, the obtained solutions consistently decrease and gradually approach the analytical solution. For the finest mesh, the relative error between the current collapse load factor and the value reported by Gaydon and McCrum [35] is merely 0.47%.

Table 1. Plate hole: the computed solutions obtained with various meshes

$\mathcal{N}_e$	55	193	747	1,690	2,923	4,601
$\mathcal{N}_{var}$	9,060	33,090	131,220	299,310	519,750	820,140
λ^+_{lm}	0.843	0.819	0.810	0.806	0.805	0.804
e (%)	5.37	2.43	1.19	0.78	0.59	0.47
CPU-Time (s)	2.25	0.66	3.04	6.44	10.18	10.18

$\mathcal{N}_e$: the number of elements; $\mathcal{N}_{var}$: the number of variables; λ^+_{lm}: the upper bound limit load factor; e: relative errors; CPU-Time: computational time for optimization problem.

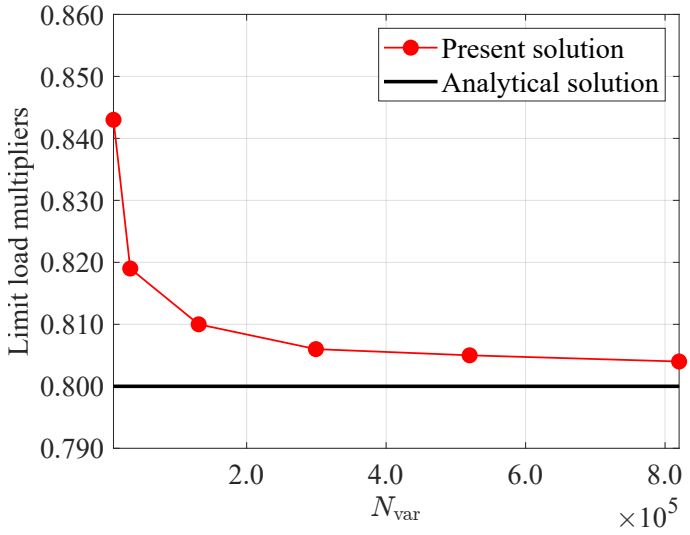

Fig. 4. Plate hole: the computed limit load multipliers versus the number of variables

In Table 1, the computational time indicates that the optimization problem can be solved quickly, taking only 10.18 seconds, utilizing second-order cone programming. This highlights the capacity of the proposed method to efficiently handle substantial engineering problems. Additionally, Fig. 5 illustrates the normalized plastic dissipation power distributions for different load combinations, offering insights into the plate's collapse mechanisms.

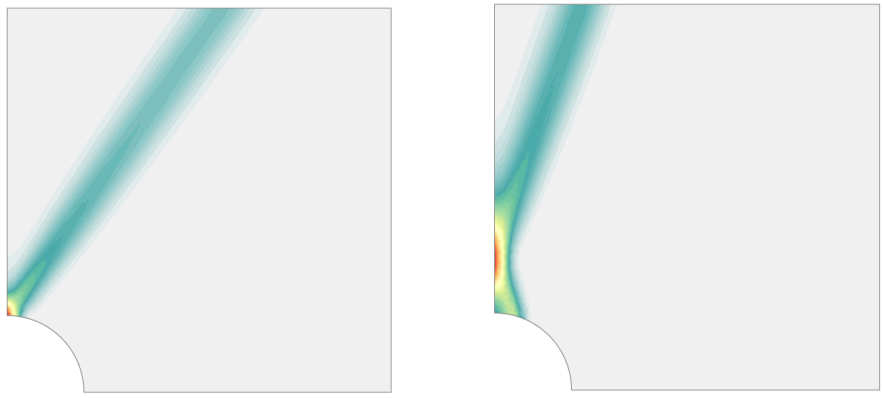

(a) $p_1 \neq 0,\ p_2 = 0$ (b) $p_1 = 2p_2$

Fig. 5. Plate hole: the dissipation power distributions for different load combinations

5.2. Plate under repeated variable loads

The effect of repeated variable pressures on the load-carrying capacity of the plate is under investigation. Interaction diagrams associated with numerous points in the loading domain are depicted in Fig. 6(a). Notably, the shakedown load envelope is considerably smaller than the collapse limits. This suggests that under the influence of repeated

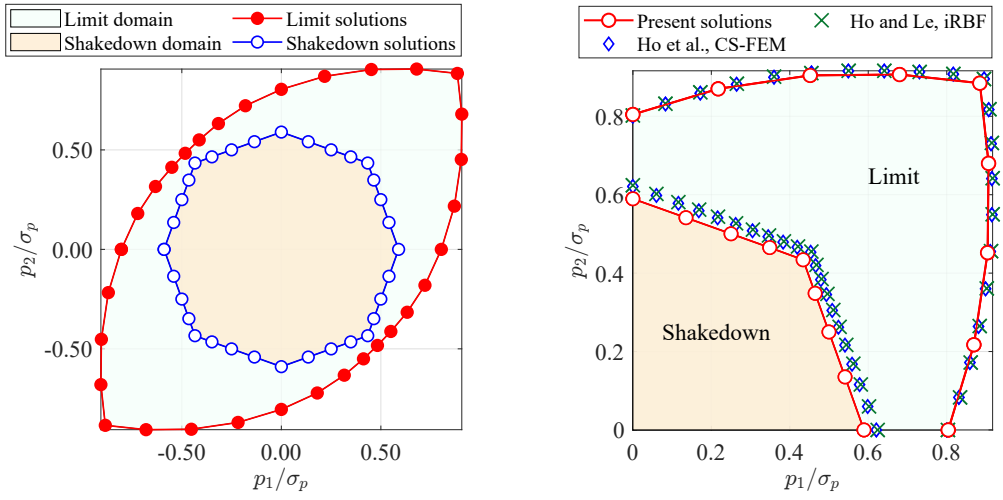

Fig. 6. Plate hole: (a) Limit and shakedown interaction diagrams;
(b) The comparison with other studies

variable external forces, the plate may lose its load-bearing capacity at load intensities significantly lower than the ultimate stress of the material.

Table 2. Plate hole: the comparison with other studies

Loading case (p_1, p_2)	λ_{lm}			λ_{sd}		
	(1, 0)	(1, 0.5)	(1, 1)	(1, 0)	(1, 0.5)	(1, 1)
Present study	0.804	0.904	0.884	0.589	0.500	0.434
da Silva and Antao [36]	0.807	0.915	0.899	-	-	-
Chen et al. [37]	0.798	0.899	0.874	-	-	-
Zouain et al. [15]	0.803	0.911	0.894	0.594	0.500	0.429
Groβ-Weege [14]	0.792	0.891	0.882	0.614	0.524	0.446
Krabbenhøft et al. [17]	-	-	-	0.595	0.499	0.430
Genna [38]	-	-	-	0.604	0.508	0.438
Tran et al. [19]	-	-	-	0.610	0.514	0.444

Fig. 6(b) illustrates a graphical comparison between the computed collapse and shakedown limits and the pseudo-lower solutions reported by Ho et al. [11] using the CS-FEM and by Ho and Le [12] using the stabilized iRBF mesh-free method. In general, our current results exhibit slightly lower values compared to those presented in [11, 12], particularly in the case of shakedown analysis. The close alignment between our findings and those obtained in previous studies, as summarized in Table 2, serves as a validation of the computational efficiency inherent to our proposed approach.

6. CONCLUSIONS

The polygonal finite element method, in conjunction with second-order cone programming, has been formulated within the context of limit and shakedown analysis applied to structural systems. This research endeavors to assess the impact of both monotonic and cyclic loading conditions on the structural load-carrying capacity. By doing so, it aims to determine the collapse and shakedown limits of structures. The numerical investigations have convincingly demonstrated that the proposed approach yields highly accurate solutions while keeping computational demands at a minimum. In future work, we intend to further enhance the efficiency of this approach by implementing various smoothing techniques, such as edge-based, cell-based, or node-based strategies. The objective is to reduce the size of the resulting optimization problem and consequently improve the computational efficiency of the current procedure.

DECLARATION OF COMPETING INTEREST

The authors declare that they have no known competing financial interests or personal relationships that could have appeared to influence the work reported in this paper.

FUNDING

This research received no specific grant from any funding agency in the public, commercial, or not-for-profit sectors.

REFERENCES

[1] W. T. Koiter. General theorems for elastic plastic solids. *Progress of Solid Mechanics*, (1960), pp. 167–221.

[2] E. Melan. Zur plastizität des räumlichen kontinuums. *Ingenieur-Archiv*, **9**, (2), (1938), pp. 116–126. https://doi.org/10.1007/bf02084409.

[3] T. Belytschko. Plane stress shakedown analysis by finite elements. *International Journal of Mechanical Sciences*, **14**, (9), (1972), pp. 619–625. https://doi.org/10.1016/0020-7403(72)90061-6.

[4] V. Carvelli, Z. Z. Cen, Y. Liu, and G. Maier. Shakedown analysis of defective pressure vessels by a kinematic approach. *Archive of Applied Mechanics*, **69**, (1999), pp. 751–764. https://doi.org/10.1007/s004190050254.

[5] A.-M. Yan and H. Nguyen-Dang. Kinematical shakedown analysis with temperature-dependent yield stress. *International Journal for Numerical Methods in Engineering*, **50**, (5), (2001), pp. 1145–1168. https://doi.org/10.1002/1097-0207(20010220)50:5<1145::aid-nme70>3.0.co;2-c.

[6] D. K. Vu, A. M. Yan, and H. Nguyen-Dang. A primal–dual algorithm for shakedown analysis of structures. *Computer Methods in Applied Mechanics and Engineering*, **193**, (42-44), (2004), pp. 4663–4674. https://doi.org/10.1016/j.cma.2004.03.011.

[7] J.-W. Simon. Direct evaluation of the limit states of engineering structures exhibiting limited, nonlinear kinematical hardening. *International Journal of Plasticity*, **42**, (2013), pp. 141–167. https://doi.org/10.1016/j.ijplas.2012.10.008.

[8] K. D. Andersen, E. Christiansen, A. R. Conn, and M. L. Overton. An efficient primal-dual interior-point method for minimizing a sum of Euclidean norms. *SIAM Journal on Scientific Computing*, **22**, (1), (2000), pp. 243–262. https://doi.org/10.1137/s1064827598343954.

[9] C. D. Bisbos, A. Makrodimopoulos, and P. M. Pardalos. Second-order cone programming approaches to static shakedown analysis in steel plasticity. *Optimization Methods and Software*, **20**, (1), (2005), pp. 25–52. https://doi.org/10.1080/10556780420002160 03.

[10] C. V. Le, T. D. Tran, and D. C. Pham. Rotating plasticity and nonshakedown collapse modes for elastic–plastic bodies under cyclic loads. *International Journal of Mechanical Sciences*, **111**, (2016), pp. 55–64. https://doi.org/10.1016/j.ijmecsci.2016.04.001.

[11] P. L. H. Ho, C. V. Le, and T. Q. Chu. The equilibrium cell-based smooth finite element method for shakedown analysis of structures. *International Journal of Computational Methods*, **16**, (05), (2019). https://doi.org/10.1142/s0219876218400133.

[12] P. L. H. Ho and C. V. Le. A stabilized iRBF mesh-free method for quasi-lower bound shakedown analysis of structures. *Computers & Structures*, **228**, (2020). https://doi.org/10.1016/j.compstruc.2019.106157.

[13] P. H. Nguyen, C. V. Le, and P. L. H. Ho. Numerical evaluation of macroscopic fatigue criterion of anisotropic materials using computational homogenization and conic programming. *European Journal of Mechanics-A/Solids*, **95**, (2022). https://doi.org/10.1016/j.euromechsol.2022.104654.

[14] J. Groβ-Weege. On the numerical assessment of the safety factor of elastic-plastic structures under variable loading. *International Journal of Mechanical Sciences*, **39**, (4), (1997), pp. 417–433. https://doi.org/10.1016/s0020-7403(96)00039-2.

[15] N. Zouain, L. Borges, and J. L. Silveira. An algorithm for shakedown analysis with nonlinear yield functions. *Computer Methods in Applied Mechanics and Engineering*, **191**, (23-24), (2002), pp. 2463–2481. https://doi.org/10.1016/s0045-7825(01)00374-7.

[16] G. Garcea, G. Armentano, S. Petrolo, and R. Casciaro. Finite element shakedown analysis of two-dimensional structures. *International Journal for Numerical Methods in Engineering*, **63**, (8), (2005), pp. 1174–1202. https://doi.org/10.1002/nme.1316.

[17] K. Krabbenhøft, A. V. Lyamin, and S. W. Sloan. Bounds to shakedown loads for a class of deviatoric plasticity models. *Computational Mechanics*, **39**, (2007), pp. 879–888. https://doi.org/10.1007/s00466-006-0076-3.

[18] H. V. Do and H. Nguyen-Xuan. Computation of limit and shakedown loads for pressure vessel components using isogeometric analysis based on Lagrange extraction. *International Journal of Pressure Vessels and Piping*, **169**, (2019), pp. 57–70. https://doi.org/10.1016/j.ijpvp.2018.11.012.

[19] T. N. Tran, G. R. Liu, H. Nguyen-Xuan, and T. Nguyen-Thoi. An edge-based smoothed finite element method for primal–dual shakedown analysis of structures. *International Journal for Numerical Methods in Engineering*, **82**, (7), (2010), pp. 917–938. https://doi.org/10.1002/nme.2804.

[20] H. Nguyen-Xuan, T. Rabczuk, T. Nguyen-Thoi, T. N. Tran, and N. Nguyen-Thanh. Computation of limit and shakedown loads using a node-based smoothed finite element method. *International Journal for Numerical Methods in Engineering*, **90**, (3), (2012), pp. 287–310. https://doi.org/10.1002/nme.3317.

[21] S. Zhou, Y. Liu, D. Wang, K. Wang, and S. Yu. Upper bound shakedown analysis with the nodal natural element method. *Computational Mechanics*, **54**, (2014), pp. 1111–1128. https://doi.org/10.1007/s00466-014-1043-z.

[22] D. W. Spring, S. E. Leon, and G. H. Paulino. Unstructured polygonal meshes with adaptive refinement for the numerical simulation of dynamic cohesive fracture. *International Journal of Fracture*, **189**, (2014), pp. 33–57. https://doi.org/10.1007/s10704-014-9961-5.

[23] S. E. Leon, D. W. Spring, and G. H. Paulino. Reduction in mesh bias for dynamic fracture using adaptive splitting of polygonal finite elements. *International Journal for Numerical Methods in Engineering*, **100**, (8), (2014), pp. 555–576. https://doi.org/10.1002/nme.4744.

[24] H. Chi, C. Talischi, O. Lopez-Pamies, and G. H. Paulino. Polygonal finite elements for finite elasticity. *International Journal for Numerical Methods in Engineering*, **101**, (4), (2015), pp. 305–328. https://doi.org/10.1002/nme.4802.

[25] E. L. Wachspress. A rational basis for function approximation. In *Conference on Applications of Numerical Analysis: Held in Dundee/Scotland, March 23–26, 1971*, Springer, Springer, (2006), pp. 223–252, https://doi.org/10.1007/BFb0069458.

[26] A. Tabarraei and N. Sukumar. Application of polygonal finite elements in linear elasticity. *International Journal of Computational Methods*, **3**, (2006), pp. 503–520. https://doi.org/10.1142/s021987620600117x.

[27] E. T. Ooi, C. Song, F. Tin-Loi, and Z. Yang. Polygon scaled boundary finite elements for crack propagation modelling. *International Journal for Numerical Methods in Engineering*, **91**, (3), (2012), pp. 319–342. https://doi.org/10.1002/nme.4284.

[28] C. Talischi, G. H. Paulino, A. Pereira, and I. F. M. Menezes. PolyTop: a Matlab implementation of a general topology optimization framework using unstructured polygonal finite element meshes. *Structural and Multidisciplinary Optimization*, **45**, (2012), pp. 329–357. https://doi.org/10.1007/s00158-011-0696-x.

[29] K. N. Chau, K. N. Chau, T. Ngo, K. Hackl, and H. Nguyen-Xuan. A polytree-based adaptive polygonal finite element method for multi-material topology optimization. *Computer Methods in Applied Mechanics and Engineering*, **332**, (2018), pp. 712–739. https://doi.org/10.1016/j.cma.2017.07.035.

[30] J. A. Koenig. *Shakedown of elastic-plastic structures*. North-Holland, (1987).

[31] N. Sukumar and E. A. Malsch. Recent advances in the construction of polygonal finite element interpolants. *Archives of Computational Methods in Engineering*, **13**, (2006), pp. 129–163. https://doi.org/10.1007/bf02905933.

[32] J. Warren. On the uniqueness of barycentric coordinates. *Contemporary Mathematics*, **334**, (2003), pp. 93–100. https://doi.org/10.1090/conm/334/05977.

[33] M. S. Floater, K. Hormann, and G. Kós. A general construction of barycentric coordinates over convex polygons. *Advances in Computational Mathematics*, **24**, (2006), pp. 311–331. https://doi.org/10.1007/s10444-004-7611-6.

[34] MOSEK ApS. *The MOSEK optimization toolbox for MATLAB manual. Version 10.0*, (2022).

[35] F. A. Gaydon and A. W. McCrum. A theoretical investigation of the yield point loading of a square plate with a central circular hole. *Journal of the Mechanics and Physics of Solids*, **2**, (3), (1954), pp. 156–169. https://doi.org/10.1016/0022-5096(54)90022-8.

[36] M. V. da Silva and A. N. Antao. A non-linear programming method approach for upper bound limit analysis. *International Journal for Numerical Methods in Engineering*, **72**, (10), (2007), pp. 1192–1218. https://doi.org/10.1002/nme.2061.

[37] S. Chen, Y. Liu, and Z. Cen. Lower-bound limit analysis by using the EFG method and nonlinear programming. *International Journal for Numerical Methods in Engineering*, **74**, (3), (2008), pp. 391–415. https://doi.org/10.1002/nme.2177.

[38] F. Genna. A nonlinear inequality, finite element approach to the direct computation of shakedown load safety factors. *International Journal of Mechanical Sciences*, **30**, (10), (1988), pp. 769–789. https://doi.org/10.1016/0020-7403(88)90041-0.